Millimeter-wave and Terahertz Devices

Academic and Research Staff
Professor Qing Hu

Graduate Students
Eralp Atmaca, Hans Callebaut, Erik Duerr, Kostas Konistis, Juan Montoya, Ben Williams

Introduction

Millimeter-wave and THz frequencies (f = 0.1-10 THz) remain one of the most underdeveloped frequency ranges, even though the potential applications in remote sensing, spectroscopy, and communications are great. This is because the millimeter-wave and THz frequency range falls between two other frequency ranges in which conventional semiconductor devices are usually operated. One is the microwave frequency range, and the other is the near-infrared and optical frequency range. Semiconductor devices which utilize the classical diffusive transport of electrons, such as diodes and transistors, have a high frequency limit. This limit is set by the transient time and parasitic RC time constants. Currently, electron mobility and the smallest feature size which can be fabricated by lithography limit the frequency range to below several hundred GHz. Semiconductor devices based on quantum mechanical interband transitions, however, are limited to frequencies higher than those corresponding to the semiconductor energy gap, which is higher than 10 THz for most bulk semiconductors. Therefore, a large gap exists from 100 GHz to 10 THz in which very few devices are available.

Semiconductor quantum-effect devices (which can be loosely termed "artificial atoms"), including both vertically grown quantum-well structures and laterally confined mesoscopic devices, are human-made quantum mechanical systems in which the energy levels can be chosen by changing the sizes of the devices. Typically, the frequency corresponding to the intersubband transitions is in the millimeter-wave range ($\Delta E \sim$ 1-4 meV) for the lateral quantum-effective devices, and THz to infrared for the vertical quantum wells. It is therefore appealing to develop ultrahigh-frequency devices, such as THz lasers utilizing the intersubband transitions in these devices.

In our group, we are systematically investigating physical and engineering issues that are relevant to devices operating from millimeter-wave to THz frequencies. Specifically, we are working on THz lasers based on intersubband transitions in quantum wells, ultrahigh-frequency heterostructure bipolar transistors based on phonon-enhanced forward diffusion, and on-chip terahertz spectrometers using ultrafast photoconductive switches.

Terahertz Lasers Based on Intersubband Transitions

Project Staff
Ben Williams, Hans Callebaut, Eralp Atmaca, and Qing Hu, in collaboration with Professor Mike Melloch at Purdue University, and Mr. John Reno at Sandia National Lab.

Semiconductor quantum wells are human-made quantum mechanical systems in which the energy levels can be designed and engineered to be of any value. Consequently, unipolar lasers based on intersubband transitions (electrons that make lasing transitions between subband levels within the conduction band) were proposed for long-wavelength sources as early as the 1970s. However, because of the great challenge in epitaxial material growth and the unfavorable fast nonradiative relaxation rate, unipolar intersubband-transition lasers (also called quantum-cascade lasers) at mid-infrared wavelengths were developed only recently at Bell Laboratories. This achievement is remarkable, but the technique used in the original quantum-cascade lasers will not be directly applicable for the longer-wavelength THz range because of two major obstacles. First, the energy levels corresponding to THz frequencies (1 THz = 4 meV) are quite narrow, so the requirements for the design and fabrication of suitable quantum wells are demanding. Because of the narrow separation between subband levels, heating and electron-electron scattering will have a much greater effect. Also, the small energy scales of THz photons make the detection and analysis of spontaneous emission (a crucial step toward developing lasers) quite difficult. Second, mode confinement, which is essential for any laser oscillation, is difficult at longer wavelengths. Conventional dielectric-waveguide confinement is not applicable because the evanescent field penetration, which is proportional to the wavelength and is on the order of several tens of microns, is much greater than the active gain medium of several microns. Currently, we are investigating to overcome these two obstacles in order to develop intersubband-transition lasers. We have made good success in generating and detecting THz emission signals and on developing a novel mode confinement method using metallic waveguide structures.
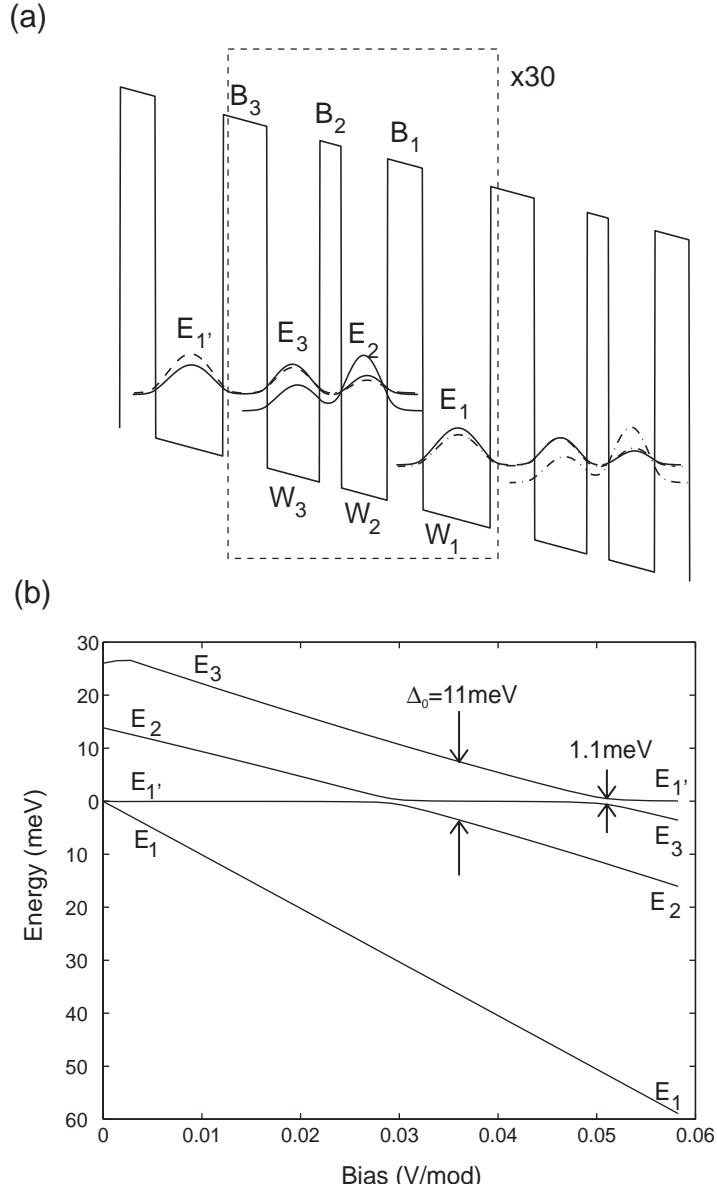
(a)

(b)

Figure 1.   Schematic of a three-level system based on a triple quantum-well structure. The radiation transition takes place between E_3 and E_2, and the fast LO-phonon emission keeps the level E_2 empty.

One of our MQW structures for THz emission is shown in Fig. 1, in which the conduction band profile and the square of the wave functions were calculated self-consistently from Schrödinger and Poisson equations. The device is formed by a triple-well structure using GaAs/Al$_{0.3}$Ga$_{0.7}$As materials, as shown in the dashed box. This structure is essentially a three-level system (marked as E_3, E_2, and E_1 in Fig. 1), which is required for any lasers. Because there is no recombination involved in unipolar intersubband lasers, electrons can be "reused" many times. Consequently, many identical triple-well modules can be cascade-connected, and the emission power and the mode confinement factor can be increased substantially. Due to translational symmetry, design analysis needs to focus only on one module, provided there are no global space charges and high-field domains. The collector barrier (the one marked as B$_1$) is center δ-doped at approximately 6×10^{10}/cm^2 in order to provide dynamic charges to assure a global charge neutrality. The radiative transition takes place between E_3 and E_2, with an energy separation of $\Delta E_{32} \approx 11$ meV (corresponding to 2.7 THz). Under the designed bias of 51 mV per module, the ground state E_1' of a previous module is aligned with E_3. Thus, the upper subband E_3 can be selectively populated through resonant tunneling. The energy separation between E_2 and E_1 was designed to be 40 meV under

3

the bias, which is slightly greater than the LO-phonon energy $\hbar\omega_{LO}$ in GaAs. Once energetically allowed, the very fast LO-phonon scattering will rapidly depopulate the E_2 level and establish a population inversion between E_3 and E_2.

In order to measure the intersubband THz emission and resolve its spectra, we constructed a set-up that included a Fourier transform infrared spectrometer (FTIR) with a composite Si bolometer as its detector. The system's schematic is shown in Fig. 2. We have improved this system and perfected our measurement techniques so that THz emission measurements can be routinely performed on our emitters with output power levels of 1-10 pW.
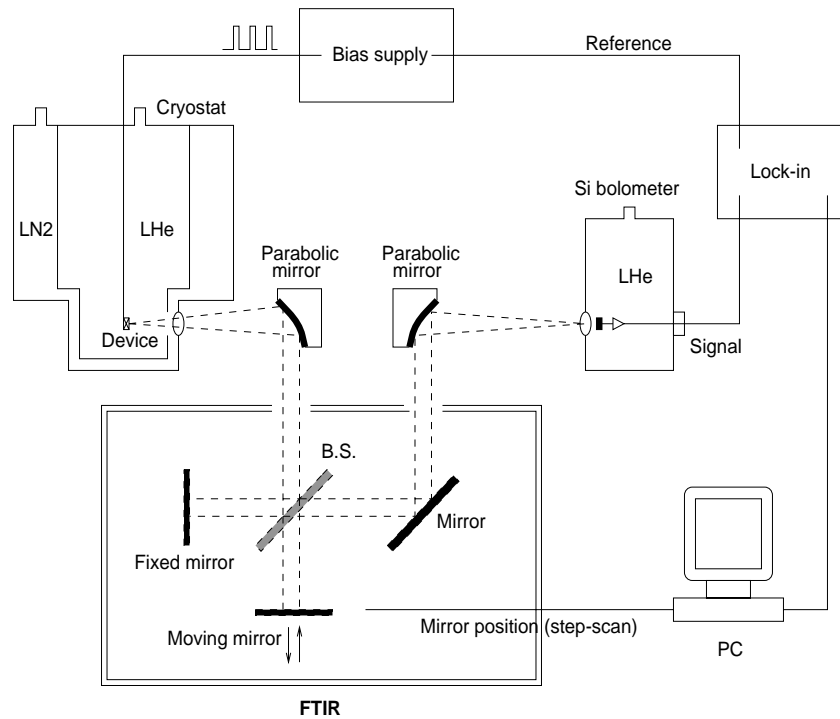

Figure 2.   Far-infrared measurement set-up that uses a Fourier transform spectrometer to spectrally resolve the emitted THz signals.

The MQW structures were grown using molecular-beam epitaxy (MBE). The emission spectra reveal a clear peak due to the $E_3 \rightarrow E_2$ intersubband emission. A representative spectrum taken at 5 K is shown in Fig. 3(a), which was taken at a bias of 1.6 V (close to the designed value of 1.53 V). The measured peak frequency of 2.57 THz (corresponding to 10.6 meV) is close to the designed value of 11 meV. The full width half maximum (FWHM) of the emission peak is as narrow as 0.47 THz (1.93 meV). Spectra were also taken with the cold stage cooled with liquid nitrogen to 80 K. A measured spectrum is shown in Fig. 3(b). The main peak is essentially the same as the one measured at 5 K, with only a slightly broader linewidth of 0.52~THz (2.14 meV). The secondary broad feature is blackbody radiation due to device heating. The linewidth measured at 80~K is expected to be similar to that at 5~K, since nonparabolicity is negligible for THz intersubband emitters. Nevertheless, our experimental verification is encouraging for the development of intersubband THz sources at elevated temperatures.
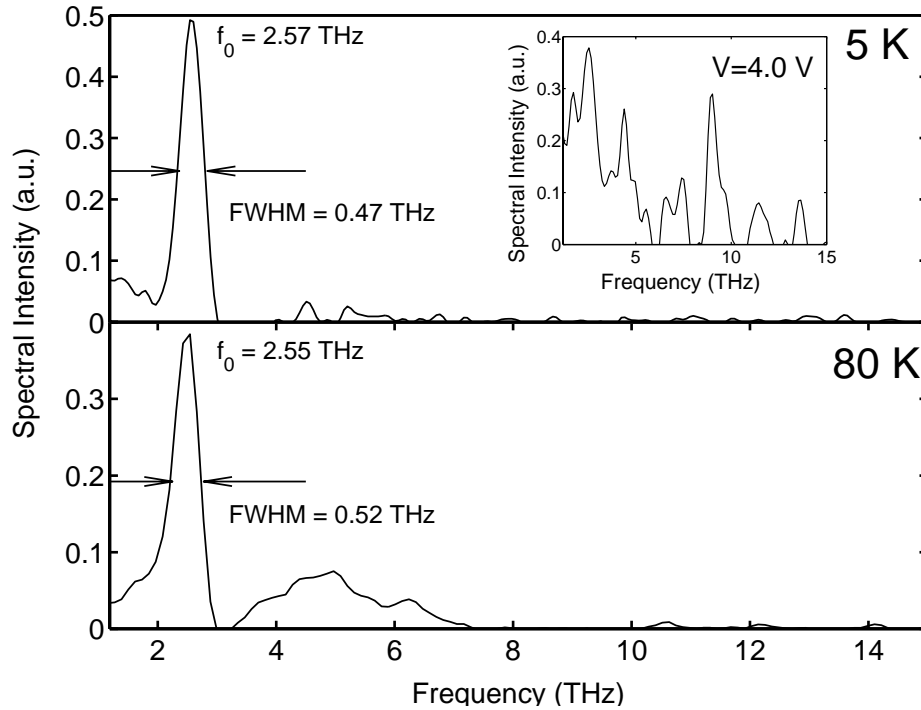
4

Figure 3.   Spectrally resolved THz intersubband emission taken at (a) 5~K and (b) 80~K under a bias of 1.6~V. The inset shows the spectrum under a 4.0~V bias.

Recently, we have designed and fabricated a new THz emission structure based on vertical (or intrawell) radiative transition, in which the radiative transition takes place between two subbands primarily located in one quantum well. The profile of the quantum-well structure is shown in Fig. 4. In this scheme, because of the strong spatial overlap of the two subband wavefunctions, the radiative transition has a large dipole moment and is less sensitive to interface roughness scattering. As a result, the radiation efficiency is higher and the emission linewidth is narrower than that of interwell transition scheme shown earlier. However, the pumping and depopulation now rely on electron-electron scattering, instead of the electron-phonon scattering as in the previous case. The analysis of electron-electron scattering is a complicated manybody problem. It becomes manageable only recently with a numerical simulation package developed by Prof. P. Harrison at University of Leeds. The structure shown in Fig. 4 was designed with the aid of this numerical code. According to our design analysis, the electron-electron scattering among the closely spaced subbands should be much faster than that between the two radiative subbands, which will yield a population inversion between the two.
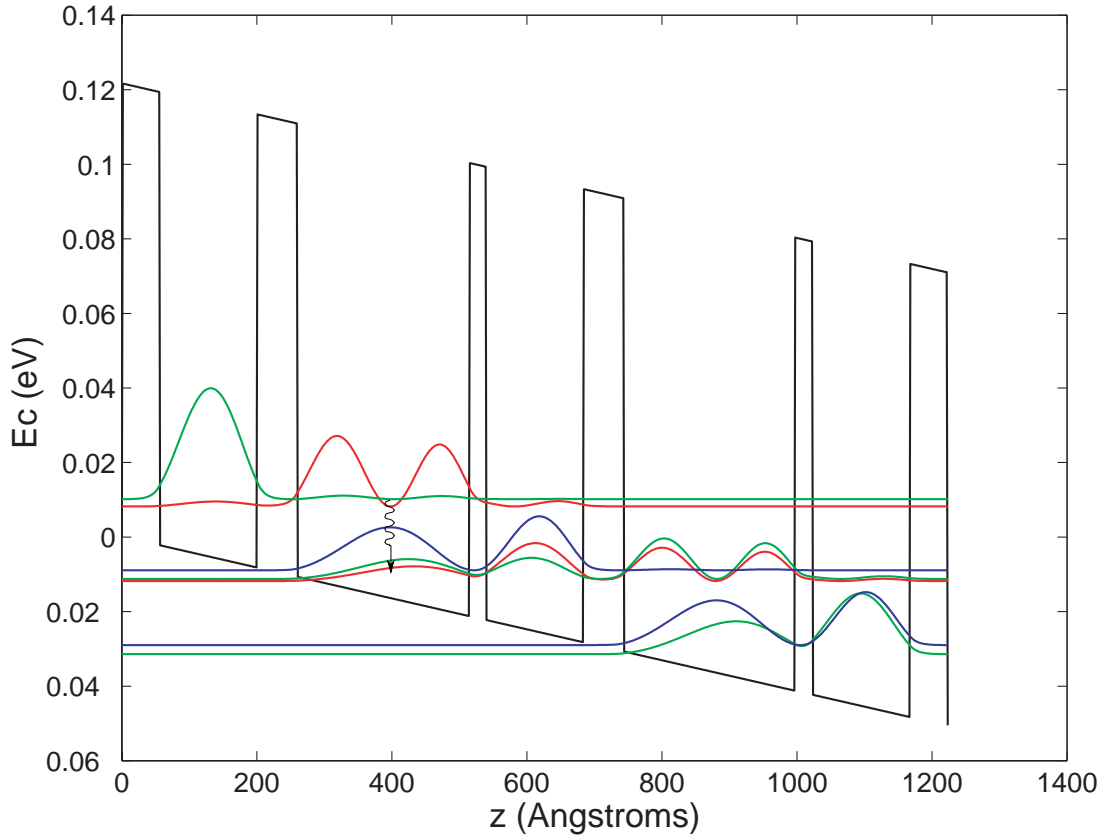
Figure 4.   Scheme of an intrawell radiative transition structure. The radiative dipole moment should be large and the emission linewidth should be narrow, due to the strong spatial overlap of the two wavefunctions. Population inversion can be facilitated by electron-electron scattering.

Our preliminary emission measurement showed very encouraging results, as shown in Fig. 5. The linewidth of the spontaneous emission is only half of that in the previous case, as expected from the intrawell scheme. Furthermore, since the fast LO-phonon scattering is not utilized in this scheme, the relaxation rate and consequently the current density is lower than those of the previous structures, yielding a much lower dc power dissipation. At this stage, we do not yet know which structure will offer the best opportunity to achieve a high degree of population inversion, and we plan to full explore both structures for the development of THz lasers.
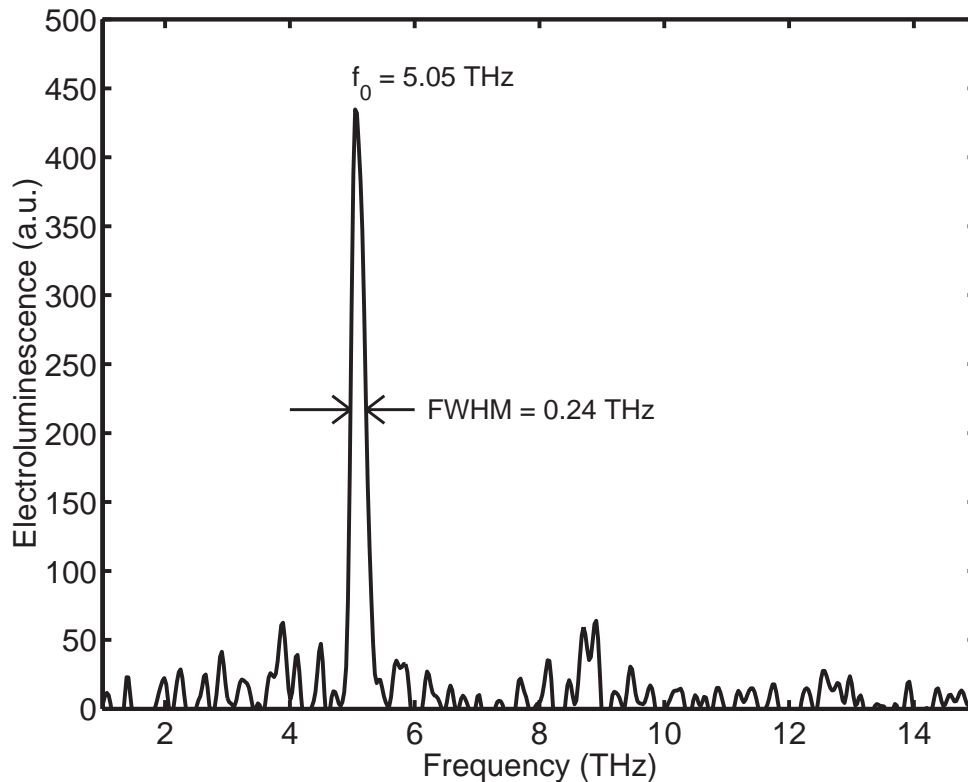
6

Figure 5.   Spectrum of spontaneous emission taken at the designed bias voltage. The center frequency is close to the designed value and the linewidth is as narrow as 1 meV (0.24 THz).

AlGaAs/GaAs HBT with enhanced forward diffusion

Sponsors
AFOSR
Grant F49620-00-1-0331

Project Staff
Kostas Konistis and Qing Hu, in collaboration with Mr. John Reno at Sandia National Lab.

One of the key limits of high-frequency operation of bipolar transistors is the base transient time, which is proportional to the square of the base width when the base transport is dominated by diffusion. Consequently, high-frequency bipolar transistors tend to use thin bases (<100 nm) that results in a short base transient time and a high cut-off frequency f_T. However, for high frequency operations, it is not the current gain that matters most. Rather, it is the unilateral power gain that determines the operating frequency of any three-terminal devices. The frequency f_{max}, at which the power gain is unity, is determined by both f_T and RC time constant. Because of the peculiar geometry of bipolar transistors, the electrical contact to the base is always made from the side. Thus, a thin base, which is important to yield a high f_T, will inevitably result in a high sheet resistance and a lowering of f_{max}. It is this difficult trade-off between f_T and f_{max} that lead Prof. S. Luryi and his co-workers to propose a novel heterostructure bipolar transistor, whose band diagram is shown in Fig. 6.
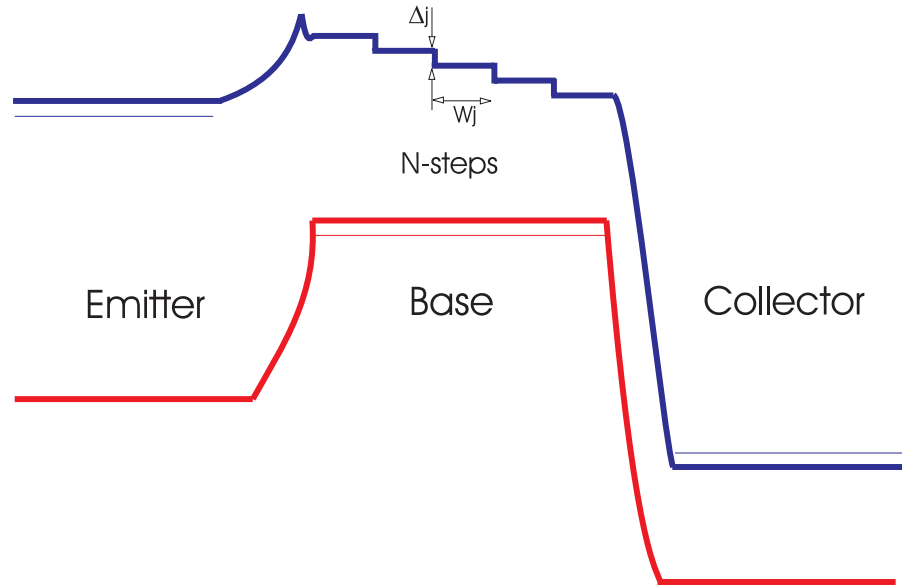
Figure 6.   Energy band diagram of an HBT with stepwise base. The energy drop Δ at each step is slightly greater than the LO-phonon energy (36 meV) in GaAs. Thus, electrons encounter very fast LO-phonon emission scattering (with a time ~0.1 ps) when they go over the edge of a step. Consequently, backward diffusion is prohibited and forward diffusion is enhanced.

The main feature of this novel HBT is that its base is graded like a staircase. The height of each step Δ is slightly greater than the LO-phonon energy in GaAs (36 meV). Thus, electrons will encounter very fast LO-phonon emission scattering (with a time ~0.1 ps) when they go over the edge of a step. Consequently, backward diffusion is prohibited. In a way, the edge of each step resembles and performs a similar function as the base-collector interface: any injected excess minority carrier will be quickly swept down the energy potential. As a result, each step acts like a minibase, as far as the diffusion transport is concerned. The resulting minority carrier concentration assumes a nearly periodic distribution provided that the energy drop is greater than the sum of LO-phonon and thermal energy to ensure a fast scattering and prohibit backward diffusion. The total base transient time is therefore approximately N times the transient time of each step, whose width can be as narrow as 30 nm, yielding a high f_T. On the other hand, all the N steps are connected in parallel for the base contact, reducing the base resistance by an approximate factor of N. The combination of a thin effective base and small base resistance will yield a high f_{max}.

The use of LO-phonon scattering as a resetting mechanism introduces the concept of independent cascade of base transport factors. In our analysis, the intrinsic part is modeled by device physics whereas the extrinsic are treated as lumped circuit elements. A simple approach that captures most of the physics is to define the transport as the product of the individual base steps assuming perfect resetting LO mechanism. As a result, the total base transport factor is a simple product of the transport factor of each step, as shown in Fig. 7. It can be seen clearly, as the number of steps N increases, the amplitude of the base transport factor increases, resulting in a higher cut-off frequency.

8

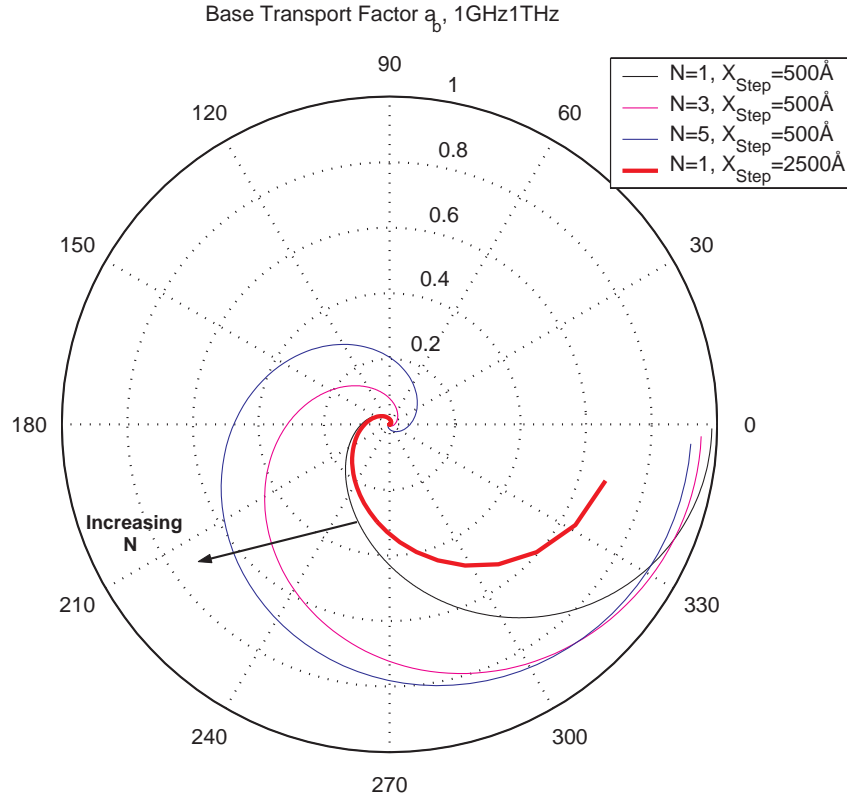Base Transport Factor a_b, 1GHz1THz

Figure 7.   Polar plot of base transport factor in frequency, for N steps and XStep step size.

One interesting result of our analysis is the existence of resonances of the unilateral power gain. Their physical mechanism is closely linked with the current-phase delay. A base structure introduces both phase delay and magnitude attenuation of current. As the frequency of operation increases, the phase delay increases and at a certain frequency the voltage and current acquire opposite phases, which will yield a resonance if the amplitude attenuation is not too overwhelming. A short base offers small phase delay and resonance occurs at high frequencies where the magnitude attenuation is strong. On the other hand, a long base may provide a large phase delay but the heavy attenuation at low frequencies smoothes out the unilateral gain peaks. For a multi-step base, the total phase delay is the sum of each step, while the total attenuation is the product of each step, enhancing the possibilities of achieving resonance. As can be seen in Fig. 7, the base transport factor of multi-step base HBTs crosses the real axis with an appreciable amplitude, Fig. 8 shows both the current gain and unilateral power gain as a function of frequency for N =1-6. Clearly, even though f_T decreases somewhat as the number of steps N increases, f_{max} barely changes due to the reduced base resistance of high-N bases. Furthermore, resonance can be achieved above 100 GHz by using multi-step base HBTs, which is promising for the development of high-frequency fundamental oscillators.
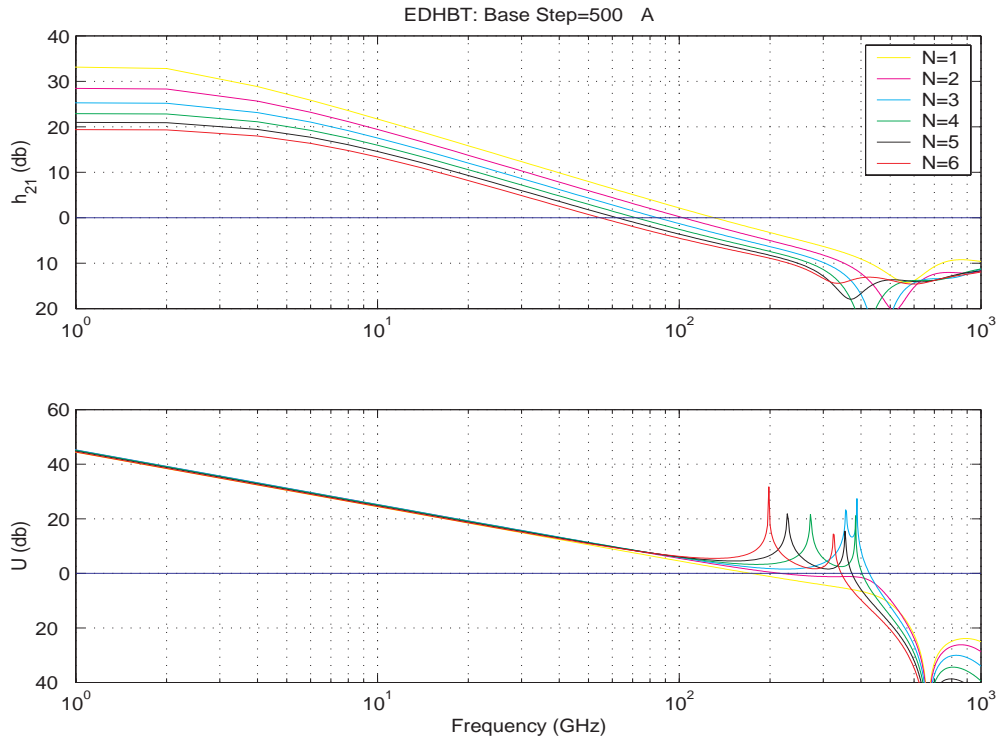
Figure 8. Current gain h_{21} and Unilateral power gain U in frequency for XStep =500 Å and variable number of steps. The resonance (peaks in U) is clearly shown above 100 GHz, which is promising for the development of high-frequency fundamental oscillators.

An on-chip frequency-domain submillimeter-wave spectrometer

Sponsor
Rosenblith Fellowship

Project Staff
Juan Montoya and Q. Hu

Because of the frequency limitation of semiconductor electronic devices, measurement instruments such as network analyzers can operate only below approximately 100 GHz. Thus, even if ultrahigh-frequency HBTs can be developed, they can only be directly measured up to 100 GHz, with higher-frequency performance extrapolated according to certain frequency roll-off models. Clearly, such an extrapolated measurement will not be applicable to measuring high-frequency resonance such as that shown in Fig. 8. It will be very useful to develop on-chip systems that can characterize device performance up to THz frequencies. A promising component for such systems is ultrafast photoconductive switches made of low-temperature-grown (LTG) GaAs materials. When pumped with two coherent laser beams, such switches can generate and detect photocurrent with a modulation frequency beyond one THz.

Furthermore, photoconductive emitters and receivers are attractive as components of sub-millimeter-wave spectroscopy systems because of their tunability, compactness and ability to be monolithically integrated with antennas, transmission lines and microelectronic devices. Such systems can be classified either as time-domain or frequency-domain systems. Time-domain systems, which contain a photoconductive pulse emitter and sampler excited by a mode-locked laser, are the most investigated. They have been used for free-space characterization of semiconductor materials, and on-chip characterization of ultrafast devices

10

and circuits with 2.7 ps time resolution. The frequency resolution is the inverse of the time span over which the propagating pulse is sampled. This span is determined by the length of an optical delay line, which usually results in a frequency resolution broader than 1 GHz.

The emitter and receiver of a frequency-domain spectrometer will be pumped by two coherent cw laser beams with frequencies ω_1 and ω_2, instead of short laser pulses. If the response time is sufficiently fast, the emitter switch will generate an ac photocurrent with a frequency $|\omega_2\text{-}\omega_1|$, which can easily exceed 1 THz. Illuminated by the same two laser beams with a controlled delay, the receiver switch can be used to perform a homodyne detection of the ac photocurrent generated from the emitter. In combination with high-frequency transmission lines, they can form on-chip spectrometers with THz bandwidths. Fig. 9 illustrates a schematic of such a spectrometer that can be used to characterize common-emitter performance of high-frequency HBTs.
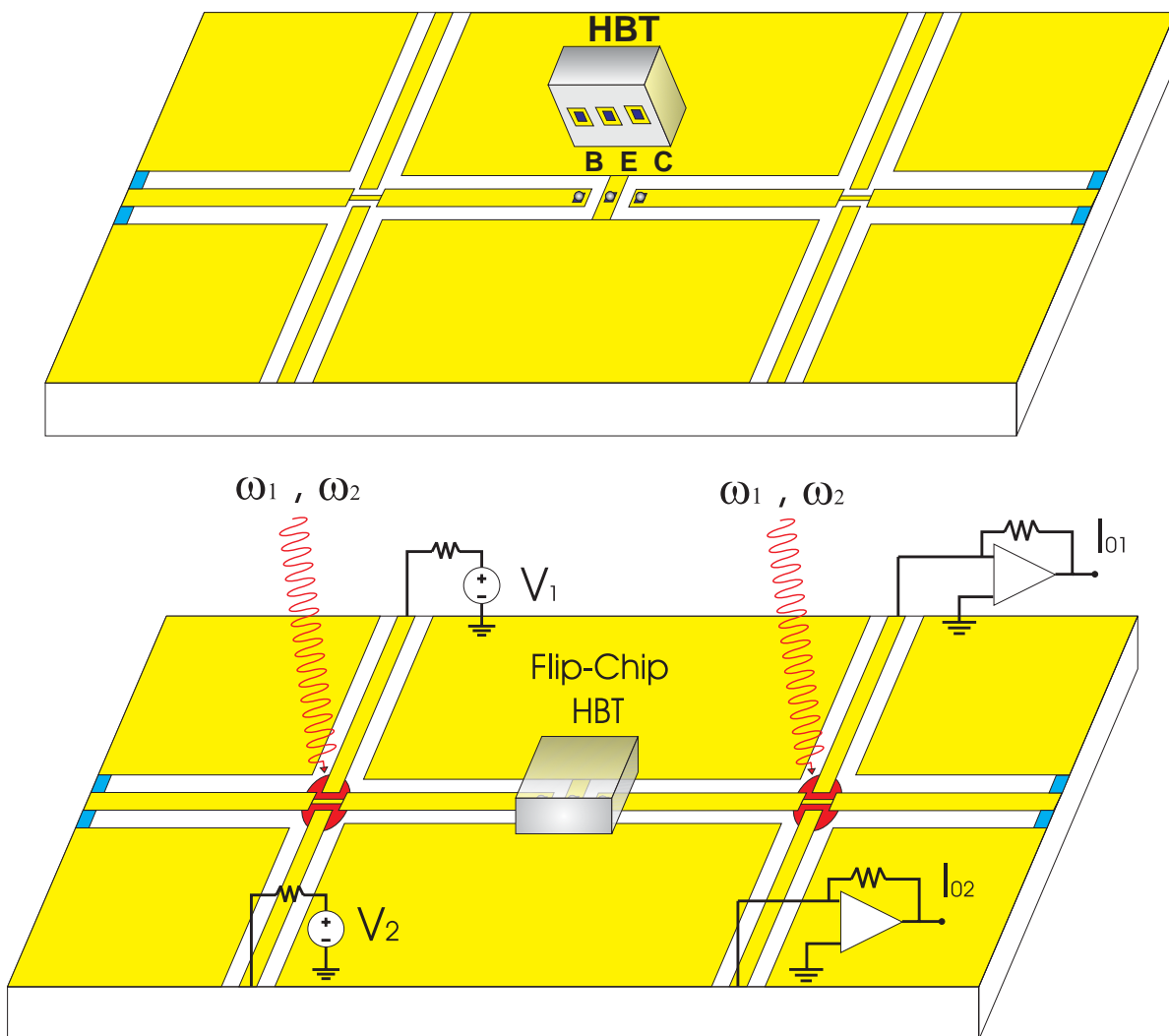

Figure 9.   Schematic of a on-chip spectrometer that uses ultrafast photoconductive switches to generate and detect ultrahigh-frequency signals.

11

Because of the broad bandwidth (>1 THz) and a high frequency resolution (better than 1 MHz), such a spectrometer is also adequate for molecular line spectroscopy. In combination with microchambers, the spectrometer can be part of a microfluidic, "lab on a chip"-type circuit, which can be used as on-chip sensors for chemical and biological agents. As the first step in the development of an on-chip frequency-domain spectrometer, we have investigated the performance of an on-chip transceiver containing only uninterrupted coplanar waveguides (CPWs).

Our circuit, shown in Fig. 10(a), has a biased pump photoconductor and an unbiased probe photoconductor connected by a main CPW, and other parasitic CPWs which provide DC electrical contact to the photoconductors. As illustrated in Fig. 10(a), we excited propagating electromagnetic waves at the pump by illuminating the pump photoconductor with two overlapping diode laser beams with a difference frequency $f = \omega_2 - \omega_1$. We performed homodyne detection of those waves by illuminating the probe with a delayed portion of the same laser beams. The relative delay between the pump and probe beams is the phase Φ. The output DC current I_{o1} should vary sinusoidally with Φ, $I_{o1}(\Phi) = I_o\cos(\Phi+\delta)$, because of the homodyne detection performed at the probe photoconductor. The argument of cosine contains two terms: the phase Φ, which is due only to the path lengths of the pump and probe beams; and the phase δ, which describes the response of the circuit and any device or specimen inserted in it. For example, δ may be non-zero because of the dispersion of the CPWs or circuit resonance. Our aim was to measure I_o and δ as functions of f. Together, I_o and δ contain all the information necessary for coherent spectroscopy.
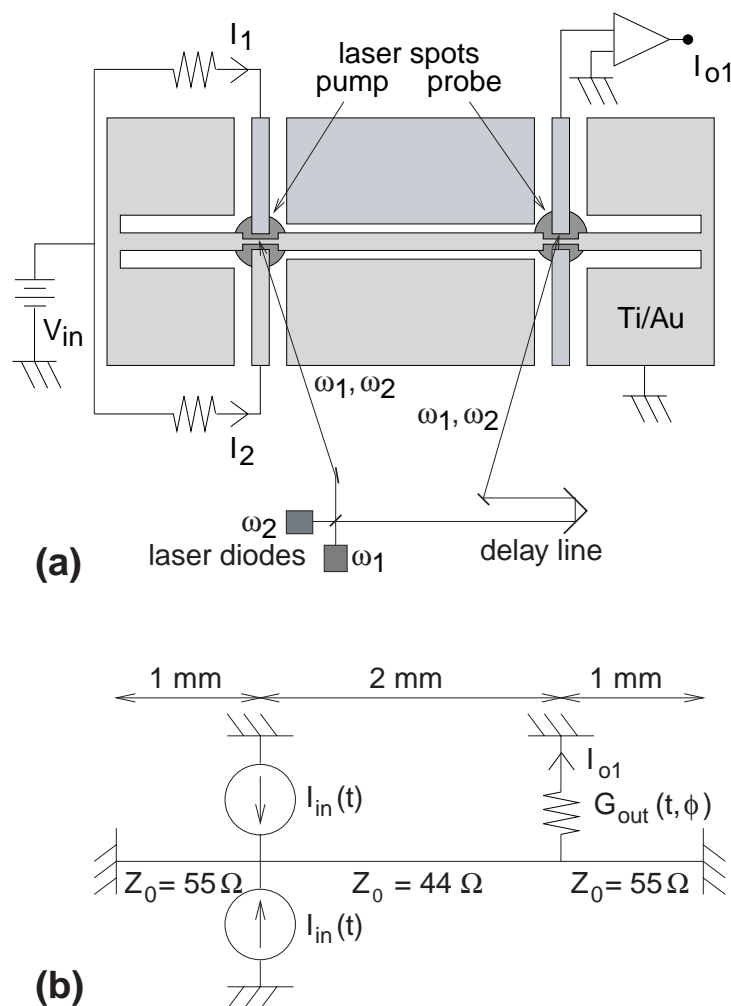

Figure 10.   (a): Diagram of the experimental circuit, showing its electrical bias and optical input. (b) Microwave circuit model of the experimental circuit.

We fit the measured spectra to a model based on the circuit shown in Fig. 10(b). The two active regions of the pump photoconductor are modeled as current sources. Similarly, the single utilized active region of the probe photoconductor is modeled as the time-varying conductance. We assume that the CPWs have a propagation constant $\Gamma = \alpha(f) + j2\pi f/v_p$, where $\alpha(f)$ is the attenuation constant to be fit to the data, and v_p is the phase velocity of a coplanar transmission line on a semi-infinite GaAs substrate. We use standard microwave circuit analysis to calculate I_{o1}, the Φ-dependent DC current generated at the probe.
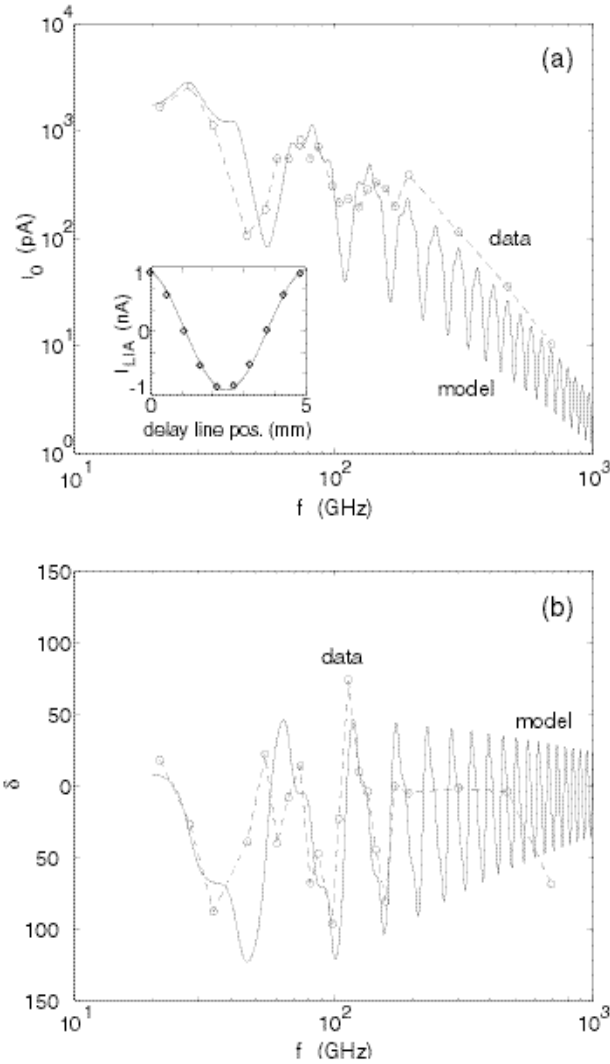

Figure 11.   Measured data and model of the amplitude and phase spectra (a) $I_o(f)$ and (b) $\delta(f)$. Inset: output of lock-in amplifier vs. delay line position at f=27.9 GHz, compared to a best-fit sinusoid.

Our model was fit to the data with reasonable fitting parameters. As shown in Fig. 11, the agreement between the model and the measured results is quite good, validating the microwave-circuit analysis of our on-chip submillimeter-wave transceiver.

Theses

MS. theses

Timpe, Jason, thesis title, Measurement and Analysis of 1/f Noise in Uncooled Microbolometers," May, 2000.